INTERNATIONAL JOURNAL OF CLIMATOLOGY, VOL. 11, 111–133 (1991) 551.513.1:551.525.2:551.579.5:551.588.3(71)

CLASS—A CANADIAN LAND SURFACE SCHEME FOR GCMS. I. SOIL MODEL

DIANA L. VERSEGHY

Canadian Climate Centre, 4905 Dufferin Street, Downsview, Ontario, M3H 5T4, Canada

Received 20 September 1989
Revised 25 April 1990

ABSTRACT

A new GCM land surface scheme is introduced, incorporating three soil layers with physically based calculations of heat and moisture transfers at the surface and across the layer boundaries. Snow-covered and snow-free areas are treated separately. The energy balance equation is solved iteratively for the surface temperature; the surface infiltration rate is calculated using a simplified theoretical analysis allowing for surface ponding. Snow cover is modelled as a discrete 'soil' layer.

The results generated by CLASS are compared with those of an older model incorporating the force–restore method for the calculation of surface temperature and a bucket-type formulation for the ground moisture. Several month-long test runs are carried out in stand-alone mode. It is shown that the surface temperature in the old scheme responds more slowly to diurnal forcing and more quickly to longer term forcing than that modelled by CLASS, while its one-layer representation of soil moisture proves incapable of reproducing changes in the surface fluxes owing to surface variations of moisture content. Finally, the lumped treatment of snow and soil in the old scheme results in an extremely fast disappearance of the snow pack under certain conditions.

KEY WORDS Land surface processes General circulation models Canadian land surface scheme Climate modelling

1. INTRODUCTION

The land surface areas of the Earth represent significant sources, sinks, and reservoirs of heat and moisture with respect to the atmosphere; the evaluation of land–atmosphere transfers of energy and water is therefore an important component of any general circulation model. In recent years, parallel to the proliferation of climate change studies using GCMs, the construction and refinement of land surface packages suitable for coupling to large-scale atmospheric models has received increasing attention. Numerous investigations have demonstrated that simulations of surface climate by GCMs are very much dependent on the formulation of their land surface schemes: e.g. with regard to the treatment of soil moisture (Mitchell and Warrilow, 1987; Meehl and Washington, 1988; Gallimore and Kutzbach, 1989) and snow cover (Washington and Meehl, 1986; Yamazaki, 1989; Barnett *et al.*, 1989).

Several second-generation land surface models, of varying complexity, have been proposed over the past decade. Some concentrate mainly on canopy processes (e.g. Sellers *et al.*, 1986; van de Griend and van Boxel, 1989) incorporating only a rudimentary soil model; these will not be discussed any further, as the focus of this paper is on the soil system. Of the remaining ones, with regard to the soil thermal regime there are two main types: those that assume $\delta T/\delta z$ to be linear between each soil layer, and therefore require multiple soil layers to adequately represent the temperature profile (e.g. McCumber and Pielke, 1981; Camillo *et al.*, 1983; Carson, 1986) and those that use a form of the force–restore method to model the temperature of a vanishingly thin surface layer and a 'restoring', subsurface layer (Deardorff, 1978; Dickinson *et al.*, 1986; Noilhan and Planton, 1989). (An exception is the GISS model (Hansen *et al.*, 1983), which assumes a quadratic variation of temperature with depth for certain heat flux calculations.) The former are usually too CPU intensive, and/or

0899–8418/91/020111–23$11.50

address too shallow a soil layer, to be used in any but short-range or meso-scale models; as for the latter, although the force–restore method has been defended for diurnal surface temperature simulations (Lin, 1980; Yee, 1988) it requires considerable modification for inhomogeneous or snow covered soils and for a time-scale of the order of years (Dickinson, 1988). For the moisture regime, models generally use two or more soil layers with Darcian flow between them (e.g. McCumber and Pielke, 1981; Camillo *et al.*, 1983; Mahrt and Pan, 1984; Abramopoulos *et al.*, 1988) or a force–restore approach (Deardorff, 1978; Hansen *et al.*, 1983; Noilhan and Planton, 1988). The latter is subject to the same criticisms as for the thermal regime, however, while models following the former strategy often fail to incorporate rigorous calculations of infiltration rates and the snowpack budget.

This paper provides an introduction to 'CLASS' (Canadian Land Surface Scheme), a three-layer, physically based land surface model that was recently developed at the Canadian Climate Centre (CCC) and which attempts to address some of the shortcomings commonly found in GCM land surface schemes. Only the sections dealing with soil processes are described here; the canopy sections will be the subject of a future paper. The new scheme is compared with the one currently in place in the CCC GCM, which like many older schemes incorporates the force–restore method for the soil thermal regime and a 'bucket' approach for the moisture regime. Finally, the predictions of the two models under bare soil conditions are contrasted for several month-long runs in stand-alone mode, using identical initial conditions and external forcing.

2. OUTLINE OF CLASS

2.1. Thermal regime

At least two layers are required to adequately reproduce the soil thermal regime: a shallow surface layer to store diurnal temperature changes and a deeper layer for annual variations. CLASS incorporates three soil layers (Figure 1), with the intermediate layer included to resolve the temperatures in the middle vegetation rooting zone. The layer depths currently used are 0.10, 0.25, and 3.75 m.

Lateral heat flow is neglected; the finite-difference form of the one-dimensional heat conservation equation is applied to each layer to obtain the change in average layer temperature $\bar{T}_i$ over a time step Δt:

$$\bar{T}_i(t+1) = \bar{T}_i(t) + [G(z_{i-1}, t) - G(z_i, t)]\frac{\Delta t}{C_i \Delta z_i} \pm S_i \tag{1}$$

where $G(z_{i-1}, t)$ and $G(z_i, t)$ are the downward heat fluxes at the top and bottom of the layer, respectively, C_i is the volumetric heat capacity of the soil, Δz_i is the layer depth, and S_i is a correction term applied in case of freezing or thawing, or the percolation of ground water (see section 2.2). G and z are both taken to be positive downward.

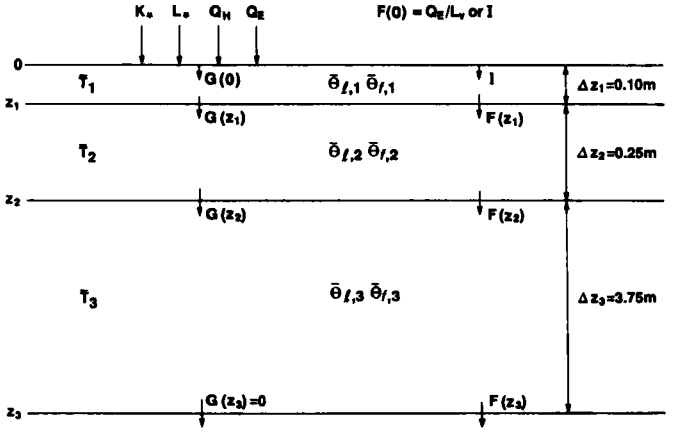

Figure 1. Schematic diagram of the structure of CLASS (see text for explanation of symbols)

The heat capacity C_i of a soil layer is calculated from the heat capacities C_j of liquid water, ice, and soil minerals present in the layer, weighted according to their respective volume fractions θ_j:

$$C_i = \sum_j (C_j \theta_j) \tag{2}$$

The thermal conductivity $\lambda(z)$, required to evaluate the heat fluxes between soil layers, is determined following the method of Johansen (1975), as recommended by Farouki (1981). The saturated thermal conductivity λ_{sat} is calculated as the geometric mean of the thermal conductivities of the soil minerals, ice, and liquid water present at the depth in question, with the relative fractions of ice and liquid water extrapolated to saturation:

$$\lambda_{sat} = \prod_j (\lambda_j^{\theta_j}) \tag{3}$$

The dry thermal conductivity is obtained from the analogous expression

$$\lambda_{dry} = \lambda_m^{(1-\theta_p)} \tag{4}$$

where λ_m is the thermal conductivity of soil minerals and θ_p is the pore volume fraction. If the soil is not saturated, $\lambda(z)$ is interpolated between its saturated and dry values according to the relative moisture content, given by the total (liquid plus ice) water volume fraction $\theta_w(z)$ at the given depth divided by θ_p:

$$\lambda(z) = [\lambda_{sat} - \lambda_{dry}]\theta_w(z)/\theta_p + \lambda_{dry} \tag{5}$$

The heat fluxes between soil layers are calculated using the known layer temperatures at each time step. These two sets of variables are related by assuming that the temperature in each layer is a quadratic function of depth. Expressions for the average layer temperatures $\bar{T}_i$ are obtained by integrating $T(z)$ over each layer. Making use of the flux-gradient relation for heat conduction in one dimension

$$G(z) = -\lambda(z)\left.\frac{dT}{dz}\right|_z, \tag{6}$$

the constraint that temperature and heat flux must be continuous across the layer boundaries, and the condition that dT/dz at the bottom of the deepest layer is zero results in a system of three linear equations in the unknown Gs, the surface temperature $T(0)$ and the known layer temperatures. Thus, if $T(0)$ is found, the heat flux terms can be evaluated.

To evaluate the surface temperature, the surface energy balance equation is expressed as a non-linear function of $T(0)$ and solved iteratively. The energy balance equation is given by

$$K_* + L_* + Q_H + Q_E = G(0) \tag{7}$$

where K_* and L_* are, respectively, the net shortwave and net longwave radiation absorbed at the surface, Q_H and Q_E are the sensible and latent heat fluxes, and $G(0)$ is the surface heat flux into the ground.

The net shortwave radiation K_* depends on the incoming shortwave radiation $K^\downarrow$ and the ground surface albedo α_g:

$$K_* = (1 - \alpha_g)K^\downarrow \tag{8}$$

The effect of solar zenith angle on the albedo of bare soils is generally small for angles less than 80°, and is ignored here. The dependence of α_g on the surface volumetric liquid water content $\theta_l(0)$ is formulated following Idso *et al.* (1975), as

$$\begin{aligned} &\alpha_g = \theta_l(0)(\alpha_{sat} - \alpha_{dry})/0{\cdot}20 + \alpha_{dry}, && \theta_l(0) < 0{\cdot}20 \\ &\alpha_g = \alpha_{sat}, && \theta_l(0) \geqslant 0{\cdot}20 \end{aligned} \tag{9}$$

where α_{sat} and α_{dry} are the limiting wet and dry soil albedoes for the given soil texture (interpolated from data given in Wilson and Henderson-Sellers (1985)). If the surface is snow covered, the snow albedo is used instead (see section 2.3).

The net longwave radiation absorbed at the surface, L_*, is given by the difference between the incoming atmospheric radiation $L^{\downarrow}$ and the radiation emitted by the surface:

$$L_* = L^{\downarrow} - \sigma T(0)^4 \tag{10}$$

where σ is the Stefan–Boltzmann constant. The surface is assumed to radiate as a black body; further refinement is a useless complication at this stage, since the effective emissivity depends not only on the measured surface value but on the effects of local microtopography.

The sensible and latent heat fluxes Q_H and Q_E are given by the bulk transfer formulae

$$Q_H = \rho_a c_p V_a c_D [T_a - T(0)] \tag{11}$$

and

$$Q_E = L_v \rho_a V_a c_D [q_a - q(0)] \tag{12}$$

where ρ_a, c_p, T_a, and q_a represent the density, specific heat, temperature, and specific humidity, respectively, of air in the constant flux layer, V_a is the wind speed, L_v is the latent heat of vaporization (or sublimation, if a snow pack is present), and c_D is a drag coefficient that depends on surface roughness length, wind speed and atmospheric stability (McFarlane and Laprise, 1985). The surface specific humidity $q(0)$ can be expressed as

$$q(0) = h \times q_{sat}[T(0)] \tag{13}$$

where h, the relative humidity of air in the surface soil pores, is given by

$$h = \exp\left[\frac{-g\psi(0)}{R_w T(0)}\right] \tag{14}$$

and $q_{sat}[T(0)]$, the saturation specific humidity at $T(0)$, is obtained from

$$q_{sat}[T(0)] = \frac{0{\cdot}622 e_{sat}[T(0)]}{p_a - 0{\cdot}378 e_{sat}[T(0)]} \tag{15}$$

In these expressions g represents the acceleration due to gravity, $\psi(0)$ is the soil-water suction at the surface (see section 2.2), R_w is the gas constant for water vapour, $e_{sat}[T(0)]$ represents the saturation vapour pressure at $T(0)$, and p_a is the surface air pressure. (If ponded water or snow is present on the surface, of course, $h = 1$.)

Finally, the system of equations in the soil temperatures and heat flux terms, described after equation (6) above, can be algebraically manipulated to yield an expression for the surface heat flux $G(0)$, which is a linear combination of the soil temperatures alone:

$$G(0) = a_1 \bar{T}_1 + a_2 \bar{T}_2 + a_3 \bar{T}_3 + a_4 T(0) + a_5 \tag{16}$$

where the a terms represent constants. If equations (8)–(16) are substituted into equation (7), therefore, the resultant expression is a function only of $T(0)$, certain atmospheric variables supplied by the GCM, and a set of known surface properties. The surface temperature $T(0)$ can thus be evaluated and substituted back into equations (8)–(16) to determine the energy balance terms, the heat fluxes between soil layers, and ultimately the layer temperatures for the next time step.

2.2. Moisture regime

The average volumetric liquid and frozen moisture contents, $\bar{\theta}_{l,i}$ and $\bar{\theta}_{f,i}$, are modelled for the same three soil layers as for the thermal regime (Figure 1), to allow coupling between soil temperature and water content. This exceeds the minimum of two soil moisture layers, found by Hunt (1985) to be essential for the generation of realistic short-term variations of surface moisture, albedo, and temperature.

The change in $\bar{\theta}_{l,i}$ over a time step is calculated using a conservation equation analogous to equation (1):

$$\bar{\theta}_{l,i}(t+1) = \bar{\theta}_{l,i}(t) + [F(z_{i-1}, t) - F(z_i, t)]\frac{\Delta t}{\Delta z_i} \tag{17}$$

where $F(z_{i-1}, t)$ and $F(z_i, t)$ represent the liquid water flow rates at the top and bottom of the layer, respectively. A change in $\bar{\theta}_{f,i}$ occurs if the predicted value of $\bar{T}_i(t+1)$ is greater than 0°C while ice is present in the layer, or if the predicted $\bar{T}_i(t+1)$ drops below 0°C while the volumetric liquid water content is greater than a limiting value of 0·04. If either condition is met, the excess energy source or sink is first used for melting or freezing, and the remainder, if any, is then used to change the temperature of the layer from 0°C. (Freezing is assumed to occur at 0°C, even though water in soil pores is known to remain liquid in small amounts down to temperatures as low as −6°C; greater accuracy in this regard is precluded by the coarse vertical resolution of the model and the lack of precise information as to the dependence of the freezing temperature range on soil texture.)

Under conditions of no precipitation, $F(0)$ is given by the surface evaporation rate $Q_E/(L_v\rho_w)$. The other $F(z_i)$ terms are evaluated using the Darcian equation for one-dimensional fluid flow:

$$F(z) = k(z)\left[\left.\frac{d\psi}{dz}\right|_z + 1\right] \tag{18}$$

where $k(z)$ represents the hydraulic conductivity at depth z and $\psi(z)$ the soil water suction (positive by convention). Water vapour movement, and liquid water movement in response to temperature gradients, are ignored. Evaporation and drainage from layers cease at a residual $\bar{\theta}_l$ of 0·04, from data presented in Mualem (1976). At the bottom of the third layer, $d\psi/dz$ is assumed to be zero, and $F(z_3) = k(z_3)$. Assuming that hysteresis and the temperature dependence of the viscosity of water are negligible, $k(z)$ and $\psi(z)$ are related to $\theta_l(z)$ and a soil texture parameter 'b' by power relations presented in Clapp and Hornberger (1978):

$$k(z) = k_{sat}\left[\frac{\theta_l(z)}{\theta_p}\right]^{(2b+3)} \tag{19}$$

and

$$\psi(z) = \psi_{sat}\left[\frac{\theta_l(z)}{\theta_p}\right]^{-b} \tag{20}$$

where k_{sat} and ψ_{sat} represent the saturated hydraulic conductivity and effective saturated soil water suction, respectively, and θ_p is the pore volume fraction. Statistically derived relationships between b, θ_p, k_{sat}, ψ_{sat}, and soil texture are presented in Cosby *et al.* (1984).

Expanding $d\psi/dz$ in terms of $\theta_l(z)$ and evaluating $d\psi/d\theta_l$ using equation (20) results in the following reformulation of equation (18):

$$F(z) = k(z)\left[\left.\frac{-b\psi(z)}{\theta_l(z)}\frac{d\theta_l}{dz}\right|_z + 1\right] \tag{21}$$

Thus, only $\theta_l(z)$ and $d\theta_l/dz|_z$ are required at the layer interfaces in order to evaluate the F terms in equation (17). For a given interface i, $\theta_l(z_i)$ is approximated as the simple arithmetic average of $\bar{\theta}_l$ in the layers above and below, and $d\theta_l/dz|_{z_i}$ is calculated as

$$\left.\frac{d\theta_l}{dz}\right|_{z_i} = \frac{\bar{\theta}_{l,i+1} - \theta_l(z_i)}{\Delta z_{i+1}} + \frac{\theta_l(z_i) - \bar{\theta}_{l,i}}{\Delta z_i} \tag{22}$$

The surface liquid moisture content $\theta_l(0)$, which is required to evaluate $\psi(0)$ and the ground albedo in section 2.1, is obtained by extrapolating $\theta_l(z)$ to the surface using $\bar{\theta}_{l,1}$ and $\theta_l(z_1)$, with the restriction that $0{\cdot}04 \leqslant \theta_l(0) \leqslant \theta_p$.

If the rainfall rate exceeds the evaporation rate and the soil is permeable, infiltration takes place at the surface; thus, $F(0) = I$, where I is the infiltration rate. (Both infiltration and evaporation are modelled as taking place if ponded water is present on the surface.) The limiting value of I for an unrestricted surface water supply, I_{lim}, is calculated after Mein and Larson (1973), who follow the classic analysis of Green and Ampt (1911) in treating the change in soil moisture due to infiltration as a downward-propagating square wave. The

expression for I_{lim} is

$$I_{lim} = \tilde{k}\left(\frac{\psi_f + z_f}{z_f}\right) \tag{23}$$

where z_f is the depth of the wetting front. The hydraulic conductivity $\tilde{k}$ behind the wetting front is estimated as $0{\cdot}5k_{sat}$ (Bouwer, 1966); $\tilde{k}$ is less than k_{sat} because as infiltration occurs a small amount of air is generally trapped in the soil. The ψ_f term represents the pressure head across the wetting front, and has been derived by Neuman (1976) and others as

$$\psi_f = \int_{\psi_{sat}}^{\psi_i} \left[\frac{k(z)}{\tilde{k}}\right] d\psi \tag{24}$$

where ψ_i is the soil water suction ahead of the wetting front, i.e. that of the layer in which the wetting front occurs. Using equations (19) and (20), equation (24) can be solved to yield:

$$\psi_f = \frac{-b\,[\psi_i k_i - \psi_{sat} k_{sat}]}{\tilde{k}(b+3)} \tag{25}$$

where k_i is the hydraulic conductivity of the layer in which the wetting front occurs. The value of ψ_f is recalculated each time z_f crosses a layer boundary.

It can be seen from equation (23) that I_{lim} decreases with increasing z_f toward an asymptotic value of $\tilde{k}$ (as long as an impermeable soil layer is not reached). Thus, if the rainfall rate $r \leqslant \tilde{k}$, the actual infiltration rate is limited by r, i.e. $I = r$. If, however, $r > \tilde{k}$, $I = r$ until the right-hand side of equation (23) becomes less than r; after this point $I = I_{lim}$ and ponding begins on the surface. The depth of the wetting front at t_p, the time of ponding, can be calculated by setting I_{lim} equal to r in equation (23) and solving for z_f. This results in

$$z_f = \frac{\psi_f}{r/\tilde{k} - 1} \tag{26}$$

If z_f is greater than the lower boundary depth of the first soil layer, the calculation is repeated for successive layers until a layer containing z_f is found or until the bottom of the soil profile is reached. In the latter case (as well as in the case where $r \leqslant \tilde{k}$), the amount of water added to the soil is $r\Delta t$. In the former case, the amount of water added to the soil up to the time of ponding is equal to $t_p r$, or $z_f(\tilde{\theta}_l - \bar{\theta}_l)$, where $\tilde{\theta}_l$ is the liquid water content behind the wetting front (corresponding to $\tilde{k}$) and $\bar{\theta}_l$ is the average initial liquid water content before the wetting front has passed. Solving for t_p using these conditions and equation (26) results in

$$t_p = \frac{\psi_f(\tilde{\theta}_l - \bar{\theta}_l)}{r\,(r/\tilde{k} - 1)} \tag{27}$$

After t_p is reached,

$$I = \tilde{k}\left(\frac{\psi_f + z_f + z_p}{z_f}\right) \tag{28}$$

where z_p is the depth of ponded water on the surface.

Ponded water is saved between time steps, rather than being dismissed as surface runoff. This approach is deemed more realistic for an area the size of a GCM grid square, little of which is generally close enough to a body of surface water to drain directly into it. (It should thus be noted that in section 4, 'runoff' in the context of CLASS refers specifically to drainage to the water table, i.e. to $F(z_3)$; in the old model, 'runoff' refers to overflow of the bucket, i.e. to overland flow.) If a pond is present, it is considered as part of the first soil layer, and the value of $\bar{T}_1$ that is saved between time steps is the weighted average temperature of the pond and the first soil layer. In this case, for the calculation of $T(0)$ above, the depth of the first soil layer is set to $\Delta z_1 + z_p$ and the thermal conductivity at the surface to that of liquid water. After $T(0)$ and the $G(z_i)$ terms have been found, $\bar{T}_1$ is decomposed into the pond and soil temperatures by solving the quadratic equation generated for the first layer. If the resultant pond temperature is less than 0°C, the energy deficit is used to freeze part or all of

the pond; the frozen water is then treated as snow. The final value of the pond temperature is used to evaluate the heat added to the soil by infiltration of water.

2.3. *Snow cover*

In CLASS, the thermal regime of snow is distinguished from that of the soil; to the best of this author's knowledge, it is the only GCM land surface scheme that does so. The snow pack is modelled as a fourth, variable-depth 'soil' layer, using the same equations for heat fluxes and the surface energy balance as in section 2.1. The heat capacity C_s of snow is calculated from C_I, the heat capacity of ice, and the densities of snow and ice ρ_s and ρ_I, respectively:

$$C_s = C_I \rho_s / \rho_I \tag{29}$$

The effective thermal conductivity of snow, λ_s, is determined from ρ_s using an equation fitted to results obtained by various researchers and presented in Mellor (1977):

$$\lambda_s = 2{\cdot}576 \times 10^{-6} \rho_s^2 + 0{\cdot}074 \tag{30}$$

where λ_s is in W m^{-1} K^{-1} and ρ_s is in kg m^{-3}. To avoid undue mathematical complexity and the need for a multilayer snow pack, snow density is assumed to be constant with depth. The magnitude of ρ_s increases exponentially with time from a fresh snow value of 100 kg m^{-3} to 300 kg m^{-3}, according to an expression derived from the field measurements of Longley (1960) and Gold (1958):

$$\rho_s(t+1) = [\rho_s(t) - 300] \exp\left[\frac{-0{\cdot}01\Delta t}{3600}\right] + 300 \tag{31}$$

where Δt is the length of the time step in seconds. Further increases in density are obtained only by refreezing of percolating melt-water or rain, which is modelled as occurring if the snow layer temperature is <0°C. After snowfalls, ρ_s is recalculated as the weighted average of the previous density and that of new snow.

The snow albedo α_s theoretically depends on grain size as well as snow density (Bohren and Barkstrom, 1974). The rate of growth of snow grains is, however, a complicated function of water vapour movement, the initial snowflake geometry, and freeze–thaw cycles. The magnitude of α_s is therefore assumed simply to decrease exponentially with time from a fresh snow value of 0·84, using an expression similar to equation (31) based on data given in Aguado (1985), Robinson and Kukla (1984) and Dirmhirn and Eaton (1975). If no melting occurs during the time step, the lower limit of α_s is 0·70:

$$\alpha_s(t+1) = [\alpha_s(t) - 0{\cdot}70] \exp\left[\frac{-0{\cdot}01\Delta t}{3600}\right] + 0{\cdot}70 \tag{32}$$

If melting occurs, the lower limit becomes 0·50:

$$\alpha_s(t+1) = [\alpha_s(t) - 0{\cdot}50] \exp\left[\frac{-0{\cdot}01\Delta t}{3600}\right] + 0{\cdot}50 \tag{33}$$

A snowfall refreshes the albedo back to 0·84. Specular reflections and the variation of α_s with solar zenith angle are ignored, as these only become important for melting or refrozen snow and for large zenith angles.

Snow is not opaque to shortwave radiation: rather, the shortwave radiation flux density decreases as an exponential function of depth, following Beer's law. The flux density K_b transmitted out of the bottom of the snow pack and assumed to be absorbed by the underlying soil is therefore calculated as

$$K_b = K_* \exp(-\kappa_s z_s) \tag{34}$$

where z_s is the depth of the snow pack and κ_s is an extinction coefficient. The latter is assigned a representative value of 20 m^{-1}, based on data presented by Grenfell and Maykut (1977) and Thomas (1963).

Melting of the snow pack can occur in two different ways. Firstly, if the solution of the surface energy balance equation results in a value of $T(0)>0$°C, this signifies that energy is available for snowmelt. In this

case $T(0)$ is reset to 0°C and L_*, Q_H, Q_E, and $G(0)$ are recomputed. The excess energy is then designated as the heat of melting, Q_M, and is used to melt a layer of snow from the top of the pack. If $\bar{T}_s(t)$, the snow layer temperature, is <0°C, the melt-water generated (as well as any rainwater that falls) percolates into the pack and refreezes at some unspecified depth, releasing latent heat and increasing the snow layer temperature and density until $\bar{T}_s(t) = 0$°C. (This process, called 'ripening' of the snow pack, is in fact observed in nature.) Thereafter, melt-water or rain-water reaches the soil surface and infiltrates or ponds, as in section 2.2.

The other way in which melting can occur is by conduction of heat from the soil underlying the snow pack, which may result in $\bar{T}_s(t+1) > 0$°C. In this case, $\bar{T}_s(t+1)$ is set back to 0°C and the excess heat is once more used to melt a layer of snow; this time, however, as the melting occurs at the bottom of the snow pack, it is supplied as 'rainfall' directly to the soil surface.

Finally, the snow cover is assumed to be complete if the snow depth is greater than an assumed surface roughness height of 0·10 m. Otherwise, the snow depth is kept fixed at 0·10 m, and the fraction of the ground surface covered, X_s, is calculated from

$$X_s = \frac{W_s}{0{\cdot}10\rho_s} \tag{35}$$

where W_s is the amount of snow present, in kg m^{-2}.

2.4. *Model organization*

At each time step and for each of the modelled grid squares, the snow temperature and the soil layer temperatures and liquid and frozen moisture contents are first retrieved from memory. The fractional snow cover is then determined using equation (35). The surface fluxes and the heat and moisture transfer rates between soil layers are calculated separately for the snow-covered and snow-free sections of each grid square. (Ponded surface water is assumed to cover grid squares uniformly.) Weighted average surface fluxes are calculated for diagnostic purposes. The layer temperatures and layer moisture contents are next stepped ahead separately for the snow-covered and snow-free sections using equations (1) and (17), with appropriate adjustments for freezing and thawing. Finally, the weighted average layer temperatures and moisture contents are calculated for each grid square and stored back into memory. The averaging is done as a surrogate for lateral transfer between snow-covered and snow-free areas; this somewhat crude approach is rendered unavoidable by the lack of detailed information on grid square topography. It can be seen, however, that despite this simplification, a first approximation to a distributed hydrological model is achieved.

The simple explicit forward-stepping scheme used in equations (1) and (17) has proved stable for the soil layer depths used and for time steps of 30 minutes or less. It has the advantage of being considerably less costly than a semi-implicit scheme, which would in this case require an iterative method of solution. The formal analysis of the truncation error associated with the forward scheme is lengthy and complicated, and will not be given here. However, some indication of the magnitude of the error that can be expected can be obtained by comparing the layer temperatures generated by the model with those given by theoretical analysis of a simple case, e.g. a homogeneous soil with a sinusoidally varying surface temperature. The analytical solution for the temperature of such a soil at time t and depth z is given (e.g. van Wijk and de Vries, 1963) as

$$T(z, t) = T_{av} + A\exp(-z/D)\sin(\omega t - z/D) \tag{36}$$

where T_{av} is the average soil temperature (constant with depth), A is the amplitude of the surface temperature variation, ω is equal to $2\pi/\tau$, where τ is the period of the temperature variation, and D is a damping depth given by

$$D = \sqrt{\frac{\lambda\tau}{\pi C}} \tag{37}$$

Equation (36) was integrated over the three soil layer depths used in the model, for a medium-textured soil at half saturation ($\lambda = 1{\cdot}50$ W m^{-1} K^{-1}, $C = 2{\cdot}2 \times 10^6$ W m^{-3} K^{-1}), and a completely dry, sandy soil

($\lambda = 0{\cdot}25$ W m^{-1} K^{-1}, $C = 1{\cdot}4 \times 10^6$ W m^{-3} K^{-1}). In both cases, $T_{av} = 15$°C, $A = 10$°C, and $\tau = 86400$ s (1 day). The temperatures of the first two layers are compared against those generated by CLASS (run to equilibrium) in Figure 2. (The temperatures of the third layer differed by an insignificant amount, and are therefore not shown.) For the medium-textured soil, temperatures differ by less than 0·25°C in the first layer and less than 0.80°C in the second layer; for the sandy soil, temperatures differ by less than 1·1°C and 0·30°C in the two layers, respectively. It would therefore seem that the errors associated with the forward-stepping scheme are relatively small.

3. OUTLINE OF PREVIOUS CCC LAND SURFACE MODEL

The model described here is the most recent version of the land surface scheme originally presented in McFarlane and Laprise (1985). Further details can be found in McFarlane *et al.* (1990).

In this scheme, the soil profile is treated as a single thermal layer. The surface temperature $T(0)$ of the layer and a restoring temperature T_r, which acts as a surrogate for subsurface temperature, are modelled using the 'force–restore' method (Deardorff, 1978). The effective soil depth D is calculated as the damping depth of the diurnal surface temperature wave, using equation (37). The soil thermal conductivity is obtained as a function of soil texture and moisture content using a set of empirical equations presented in Dickinson *et al.* (1986); the soil heat capacity is calculated as in CLASS, using equation (2).

The value of T_r is estimated as the average of $T(0)$ over the past 24 h:

$$T_r(t+1) = T_r(t) + [T(0, t+1) - T_r(t)]\,\Delta t/\tau \tag{38}$$

where $\tau = 86400$ s. Assuming diurnally periodic surface forcing, the change in $T(0)$ over a time step can be derived as

$$T(0, t+1) = T(0, t) + \frac{2G(0, t)\,\Delta t}{C_e} - \frac{2\pi\Delta t}{\tau}\left[T(0, t) - T_r\right] \pm S \tag{39}$$

where C_e, the effective heat capacity of the soil, is equal to $C \times D$. The second term on the right is the 'forcing' term, a function of the ground heat flux $G(0, t)$; the third term is the 'restoring' term, tending to drive $T(0)$ back to T_r; and the last is a source/sink term due to freezing and thawing, calculated in the same way as for CLASS above. The value of $G(0, t)$ is determined by solving the energy balance equation using $T(0, t)$; thus, the calculation of $T(0)$ for a given time step is based on an extrapolation using the surface energy fluxes of the previous time step. The energy balance terms K_*, L_*, and Q_H and their associated variables are obtained in the same way as in CLASS, except for the ground albedo, which varies in a linear fashion over the whole range of volumetric liquid moisture content $\bar{\theta}_l$:

$$\alpha_g = m_1 - m_2\bar{\theta}_l \tag{40}$$

where m_1 and m_2 are constants depending on soil texture. The value of Q_E is calculated as the product of an evaporation efficiency parameter β and the potential evapotranspiration:

$$Q_E = \beta L_v \rho_a V_a c_D [q_a - q_{sat}[T(0)]] \tag{41}$$

where L_v, ρ_a, V_a, q_a, c_D and $q_{sat}[T(0)]$ are as defined in section 2.1. For bare soil, β is parametrized as

$$\begin{aligned} \beta &= \frac{\bar{\theta}_l + \bar{\theta}_f}{0{\cdot}75\theta_p}, & (\bar{\theta}_l + \bar{\theta}_f) &< 0{\cdot}75\theta_p \\ \beta &= 1, & (\bar{\theta}_l + \bar{\theta}_f) &\geqslant 0{\cdot}75\theta_p \end{aligned} \tag{42}$$

where $\bar{\theta}_f$ is the frozen water content of the modelled soil moisture layer and θ_p is the pore volume fraction.

The soil moisture regime is simulated using a 'bucket' model. The depth of the layer modelled varies with ground cover, and is set to 0·5 m for bare soil. No drainage occurs from the bottom of the layer; gains and losses of moisture take place only at the surface, by infiltration of rain-water or melt-water and evaporation.

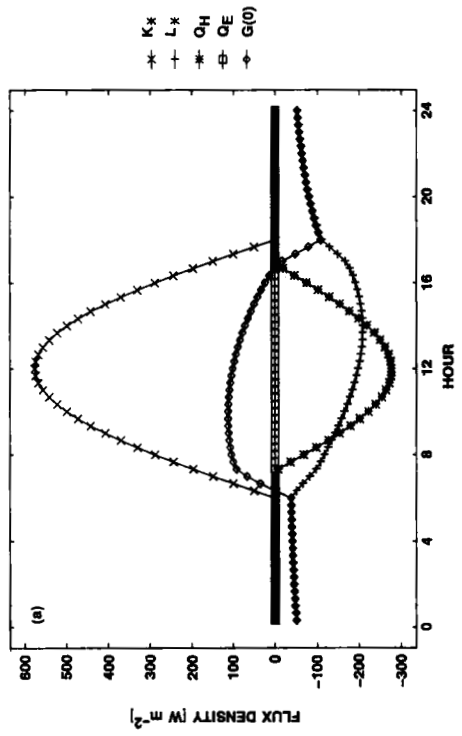

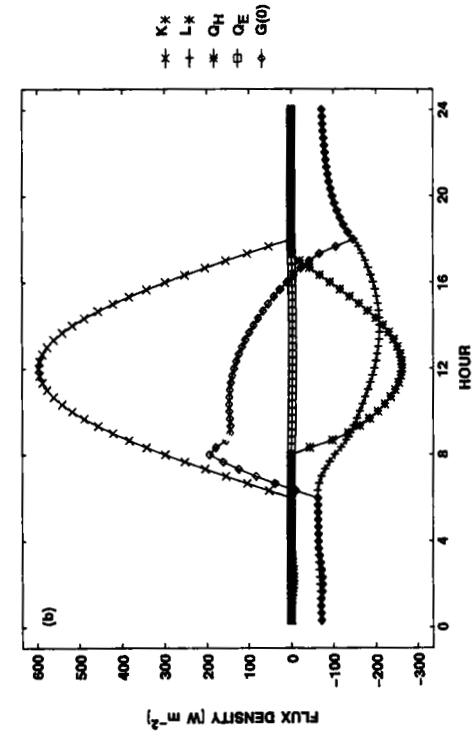

Figure 3. Run 1—Energy balance terms for the last day: (a) CLASS; (b) old scheme

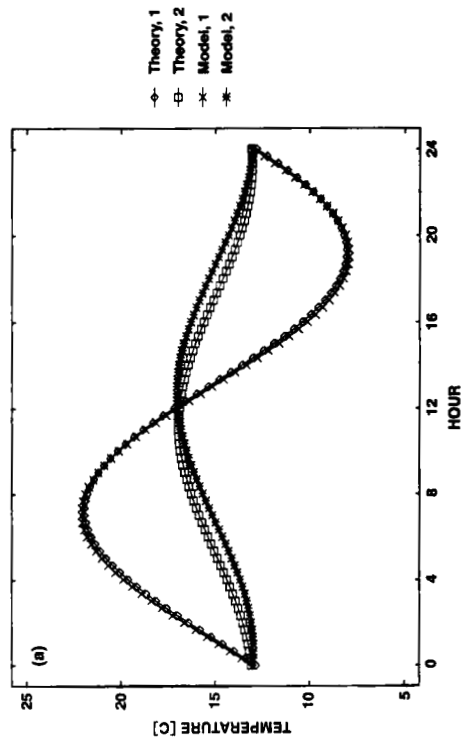

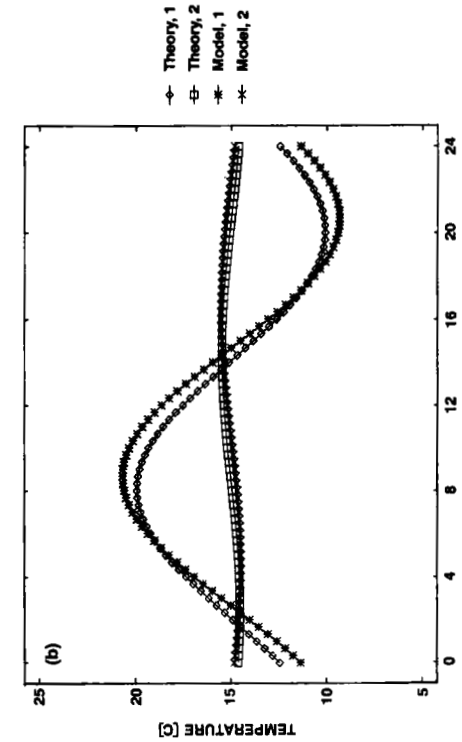

Figure 2. Comparison of first two soil layer temperatures given by theoretical analysis and by the forward-stepping scheme used in CLASS, for a homogeneous soil with sinusoidally varying surface temperature: (a) medium-textured, half-saturated soil; (b) dry, sandy soil

The infiltration rate is not explicitly modelled; any surface water generated is added to the soil moisture store until $\bar{\theta}_l = \theta_p - \bar{\theta}_f$. Further rainfall causes the bucket to 'overflow', i.e. the excess is considered to be runoff.

Snow cover is not modelled explicitly. The amount of snow W_s increases if snow falls, but melting of the snow is not separated from melting of frozen groundwater; the heat of melting Q_M is partitioned between the two according to the fractional snow cover X_s. The latter is assumed to reach 1 when the snow amount exceeds 10 kg m^{-2}; otherwise,

$$X_s = \sqrt{W_s/10{\cdot}0} \tag{43}$$

If snow is present, the effective heat capacity C_e of the ground in equation (39) is recalculated as the average of the effective snow and soil heat capacities, weighted according to X_s:

$$C_e = C_s D_s X_s + CD(1 - X_s) \tag{44}$$

The effective snow heat capacity $C_s D_s$ is assumed to have a constant value of $9{\cdot}6 \times 10^4$ J m^{-2} K^{-1}.

The snow albedo α_s decreases from 0·75 to 0·57 as a linear function of an aging factor A_s:

$$\alpha_s = 0{\cdot}75 - 0{\cdot}18A_s \tag{45}$$

The value of A_s varies between 0 for fresh snow and 1 for old snow, as

$$A_s(t+1) = A_s(t) + \frac{\Delta t}{40\tau}[1 - 2\Delta W_s(t)] \tag{46}$$

where ΔW_s is the change in snow amount owing to precipitation over the past time step. The resultant average ground albedo $\bar{\alpha}$ is calculated as

$$\begin{aligned} \bar{\alpha} &= \alpha_g + \frac{W_s}{\rho_s d_m}[\alpha_s - \alpha_g], \qquad & W_s/\rho_s < d_m \\ \bar{\alpha} &= \alpha_s, & W_s/\rho_s \geqslant d_m \end{aligned} \tag{47}$$

where d_m, the snow masking depth, is set at 0·01 m for bare soil and the snow density ρ_s is a simple linear function of W_s, with an upper limit of 450 kg m^{-3}:

$$\rho_s = 188{\cdot}82 + 0{\cdot}41931\, W_s \tag{48}$$

4. RESULTS OF STAND-ALONE TEST RUNS

Several month-long test runs were carried out, for the purpose of intercomparing the soil surface fluxes and variations of temperature and soil water content generated by the two models. The models were run in stand-alone mode, using identical surface forcing and ground initial conditions. The time step used was 1200 s. Incoming shortwave radiation, air temperature, and wind speed were specified as varying sinusoidally with a diurnal period; incoming longwave radiation and air pressure were assigned constant values of 300 W m^{-2} and 100 kPa respectively. Soil temperatures and liquid and frozen moisture contents were initialized as constant with depth; a medium-textured, clay loam soil was assumed. A summary of the variables used in the four runs discussed in this paper is given in Table I.

4.1. Run 1: Desert conditions

The first run simulates desert-like conditions, with high air temperatures and incoming shortwave radiation, and a soil dried to its residual water content. This demonstrates the temperature response of the two models without the complication of moisture movement. From Figure 3, which illustrates the energy balance terms for the last day of the month, it can be seen that the model results are broadly similar. There are, however, noticeable differences between the predicted magnitudes of $G(0)$. The old scheme produces a value of

Table I. Atmospheric forcing and soil initial conditions specified for the test runs

	Run 1	Run 2	Run 3	Run 4
Atmospheric variables				
Maximum $K^{\downarrow}$ (W m^{-2})	800	600	400	500
Diurnal T_a range (°C)	10–30	10–20	−20 to −5	5–20
Diurnal V_a range (m s^{-1})	1–5	1–5	1–5	1–5
Relative humidity (per cent)	25	75	75	75
Rainfall (mm)	0	15	0	0
Soil initial data				
$\bar{T}$ (°C)	5	5	0	0
$\bar{\theta}_l$ (volume fraction)	0·04	0·30	0·30	0·04
$\bar{\theta}_f$ (volume fraction)	0·00	0·00	0·00	0·26
Snow amount (kg m^{-2})	0	0	40	40
Soil properties held constant for all runs				
$\alpha_{sat}=0{\cdot}15$; $\alpha_{dry}=0{\cdot}27$				
$\lambda_{sat}=1{\cdot}7$ W m^{-1} K^{-1}; $\lambda_{dry}=0{\cdot}27$ W m^{-1} K^{-1}				
$k_{sat}=6{\cdot}0\times10^{-6}$ m s^{-1}				
$\psi_{sat}=0{\cdot}138$ m				
$\theta_p=0{\cdot}45$				
$b=7{\cdot}5$				

$G(0)$ that is 90 W m^{-2} greater than that given by CLASS at 0800 h, and which remains about 40 W m^{-2} greater until mid-afternoon. Overnight, the difference between the two averages more than 20 W m^{-2}.

The reason for the more extreme values of $G(0)$ associated with the old model seems to be that $T(0)$ is slow in responding to short-term surface forcing. Part of this damping effect is due to the fact that $T(0, t)$ is calculated on the basis of the surface fluxes from the previous time step. In addition, comparing the soil temperatures generated by the two models (Figure 4), it can be seen that the amplitude and phase of T_r actually follow more nearly those of the second layer temperature $\bar{T}_2$ in CLASS, than those of $\bar{T}_1$, the temperature of the soil layer most closely coupled with the surface. The restoring temperature T_r therefore has a strong restraining effect on $T(0)$, causing it to remain lower than T_a for longer in the morning. Stable conditions are thus prolonged, and the normal increase of Q_H is suppressed until 0800 h. (This is not a peculiarity of the CCC GCM; a similar anomalous lag in the sensible and latent heat fluxes and an early peak in $G(0)$ are found in the results of other force–restore based models compared with observations, e.g. in Noilhan and Planton (1989).) During the suppression of Q_H, $G(0)$ rises sharply until $T(0)$ increases to $> T_a$. Subsequently, the damping of $T(0)$ persists, resulting in a general underestimation of Q_H during the day and an overestimation of L_* at night. It is interesting to note that in another run, for which the results are not shown here, it was found that for strong heating over a moist surface the sharp peak and subsequent drop in $G(0)$ caused fluctuations of $T(0)$ above and below T_a, giving rise to wild oscillations of Q_H and Q_E ranging from weak fluxes toward the surface to strongly negative fluxes of the order of several hundreds of W m^{-2}.

Finally, although $T(0)$ reacts relatively slowly to diurnal forcing, it can be seen from Figure 5 that it reacts comparatively quickly to longer term forcing. Because T_r is calculated from an accumulated surface temperature, it soon converges to the daily average of $T(0)$; and because T_r therefore has no memory of weather further in the past than a few days, the daily average of $T(0)$ reaches an equilibrium value slightly above T_a within a month. In contrast, CLASS has three intercoupled subsurface soil layers, of which the first and third lower layer boundaries are chosen to approximate the penetration depths of the diurnal and annual temperature waves, respectively. The damping effect of the slowly moving third soil layer temperature causes the daily average surface temperature predicted by CLASS to persist at a value more than 2°C below T_a by the end of the month.

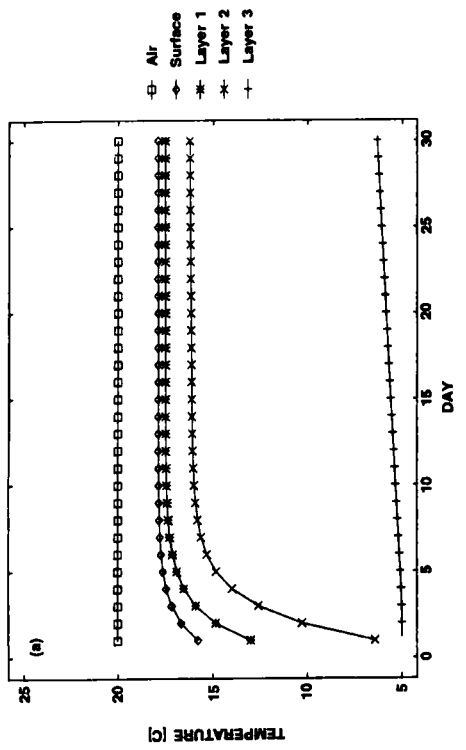

Figure 5. Run 1—Daily average soil and air temperatures: (a) CLASS; (b) old scheme

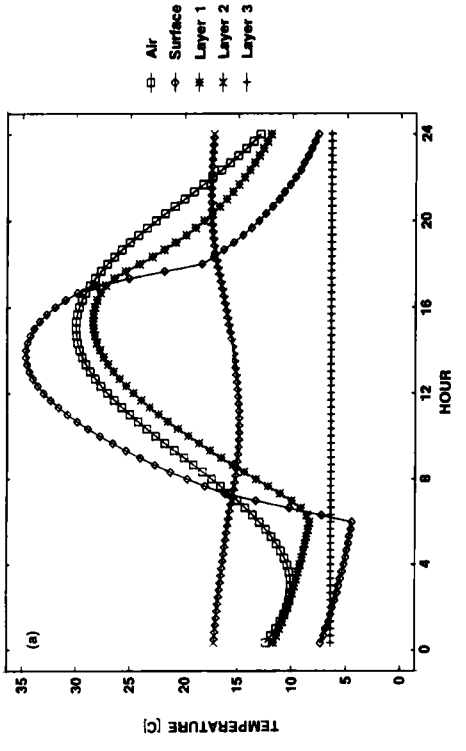

Figure 4. Run 1—Soil and air temperatures for the last day: (a) CLASS; (b) old scheme

4.2. Run 2: Rain followed by drying

The second run illustrates the differences between the two models' treatment of evaporation and soil moisture movement. On the first day of the simulated month a rainfall of 15 mm occurs, the intensity of which is not great enough to cause surface ponding. During the precipitation event, the prescribed incoming shortwave radiation is cut in half, and the relative humidity is specified as 100%. Figure 6 illustrates the changes in soil moisture storage over the month. For CLASS, the infiltration of rain-water leads to an increase in the moisture content of the first layer on the first day, and of the second layer on the first and second days as percolation occurs from above. Thereafter $\bar{\theta}_l$ of the two layers decreases as percolation to depth continues and evaporation depletes the top layer. The value of $\bar{\theta}_l$ for the third layer shows a negligibly small net change, owing to the magnitude of its storage capacity and the fact that $d\psi/dz$ reverses its sign midway through the month. As shown in Figure 7, runoff, i.e. drainage from the bottom of the third layer, persists at an almost constant rate throughout the month. Evaporation, however, drops off sharply on the ninth day, when it begins to be limited by moisture availability in the first layer. For the rest of the month, the evaporation rate and thus the rate of moisture loss to the top layer are small. Percolation from the top layer is also small, but continues to deplete the water in the second layer.

In contrast, the old scheme predicts a steady decrease of $\bar{\theta}_l$ in the single soil moisture layer, with no runoff and an almost constant evaporation rate. No runoff occurs because the bucket does not 'overflow' during the rainfall event; the evaporation rate remains high throughout the month because the evaporation efficiency parameter β is calculated on the basis of the moisture content of the entire soil layer, which reacts slowly to drying. The relative magnitudes of runoff and evaporation are thus inverted between the old scheme and CLASS: the old scheme generates a runoff of zero, compared with a value of 11 mm for CLASS, and a total evaporation of 60 mm, compared with only 17 mm for CLASS.

The effects of the differences in the treatment of soil moisture on the daily average surface energy balance terms produced by the two models can be seen in Figure 8. In the old scheme, K_* remains almost constant after the first, overcast day, because the albedo is dependent on the slowly moving θ_l. The value generated by CLASS is 8 W m^{-2} higher for the first few days and 7 W m^{-2} lower for the rest of the month. For the old scheme, L_* reaches a constant value and $G(0)$ reaches zero within 10 days, the time it takes for $T(0)$ and T_r to attain their equilibrium value of 1°C below T_a. The values of L_* and $G(0)$ produced by CLASS are smaller by up to 8 W m^{-2} and 20 W m^{-2}, respectively, than those of the old scheme during the first week, because the high evaporation rate acts to damp $T(0)$. Subsequently, the two L_* values are almost the same, because although the modelled diurnal temperature range is greater for CLASS, the two diurnal average surface temperatures coincide. At the same time, $G(0)$ for CLASS is non-zero, because the vertical temperature gradient approaches zero far more slowly than in the old scheme, owing to the multiple soil layers. The most striking differences between the model results, however, occur in Q_H and Q_E. As indicated above, both models initially generate large values of Q_E. For the latter part of the month, however, while Q_E remains around 60 W m^{-2} for the old scheme, it falls to almost zero for CLASS. The value of Q_H conversely starts out well under 10 W m^{-2} for both models, but increases to over 55 W m^{-2} for CLASS parallel to the decrease in Q_E. Thus, for 3 weeks of the modelled month, the old model predictions of Q_H and Q_E are actually the opposite of those given by CLASS.

4.3. Run 3: Fresh snow on unfrozen ground

This run was carried out to determine the effect of snow cover and soil freezing on the performance of the two models. Temperatures were initialized at 0°C, all soil moisture being specified as unfrozen, and a snow cover of 40 kg m^{-2} was added with the density and albedo of fresh snow. Figure 9 shows the temperatures generated by CLASS over the month. The first soil layer gradually freezes between day 1 and day 8, and the second layer between day 8 and day 15, after which their temperatures begin to decrease. The third layer, because of its thickness, does not freeze completely at all within the month. The snow temperature remains at a steady value of −6°C while the first soil layer is freezing, and decreases progressively thereafter as the temperature of the latter decreases. The surface temperature actually increases over the month, with slight

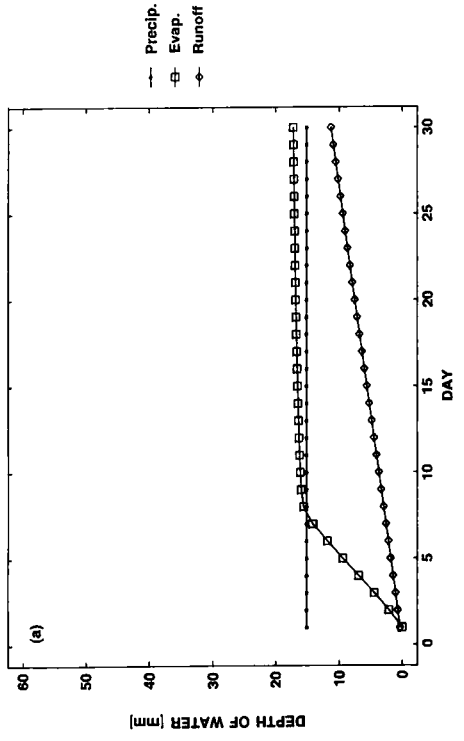

Figure 7. Run 2—Cumulative values of hydrological terms: (a) CLASS; (b) old scheme

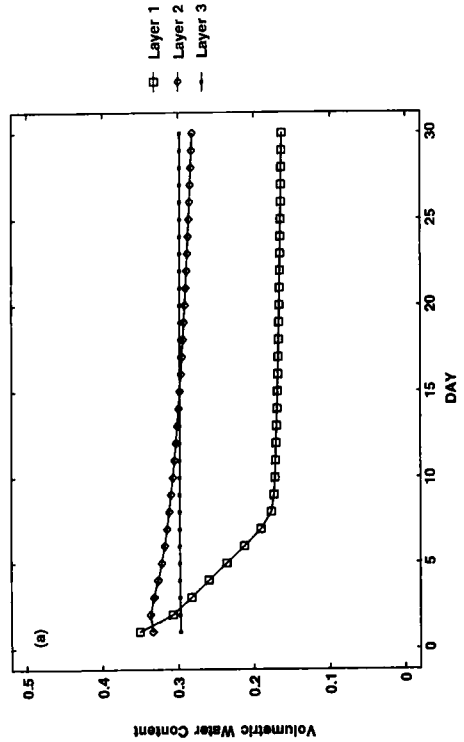

Figure 6. Run 2—Variations in soil water content: (a) CLASS; (b) old scheme

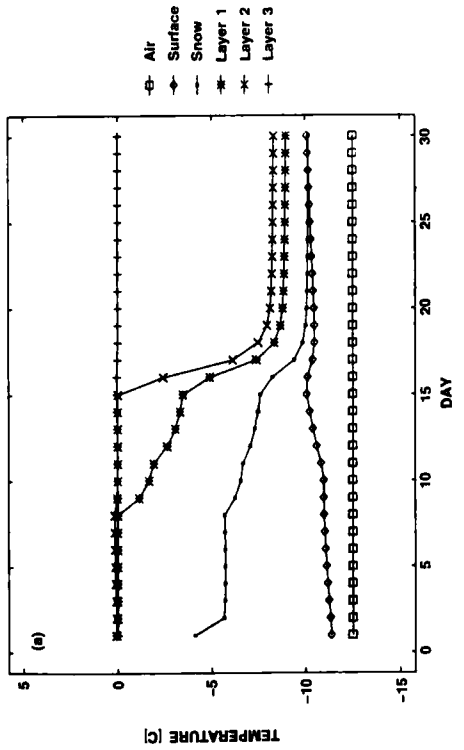

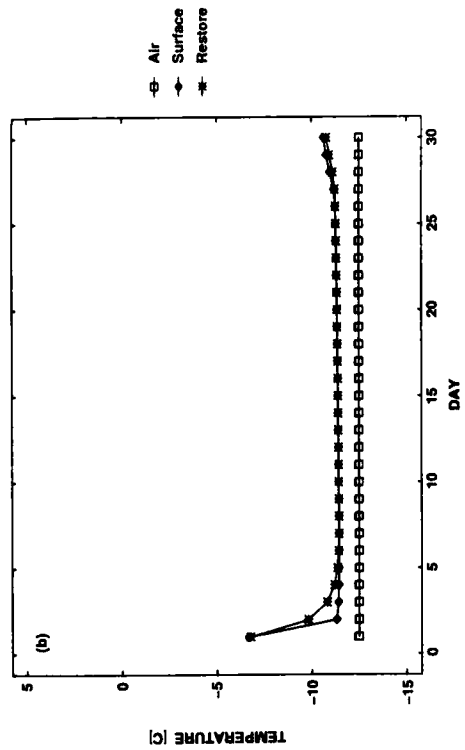

Figure 9. Run 3—Daily average soil and air temperatures: (a) CLASS; (b) old scheme

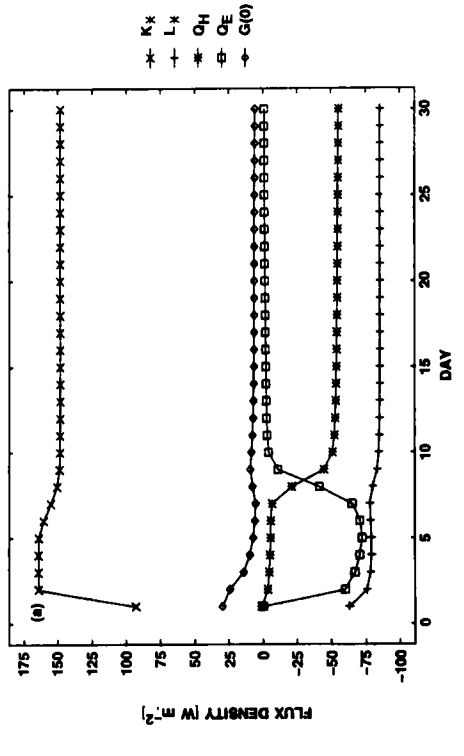

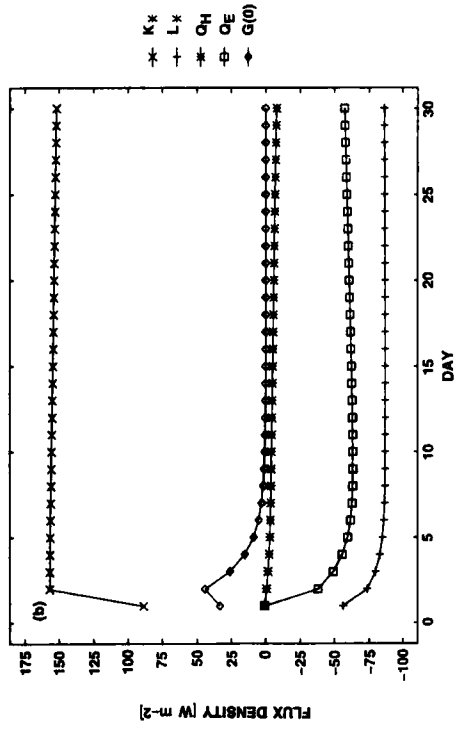

Figure 8. Run 2—Daily average energy balance terms: (a) CLASS; (b) old scheme

reversals as each soil layer freezes, because as the snow pack ages its density and thermal conductivity increase and its albedo decreases; $T(0)$ thus responds to enhanced subsurface conduction and surface heating. In addition, the fractional snow cover X_s falls below 100 per cent on the tenth day of the month, exposing the relatively warm soil over more and more of the modelled area.

For the old scheme, however, all of the water in the soil layer freezes within the first day. This is because $T(0)$ remains at 0°C as long as freezing is proceeding; thus, strongly unstable conditions persist until all of the soil water is frozen, with average values of Q_H, Q_E, and $G(0)$ on the first day reaching magnitudes of 450, 250, and 650 W m^{-2}, respectively. Within the first week $T(0)$ and T_r reach their equilibrium value of 1°C above T_s. The effect of this quick freezing response on the modelled hydrological terms is shown in Figure 10. Owing to the high evaporation rate on the first day of the run, the snow pack drops by almost 8 kg m^{-2} (= mm of liquid water equivalent). Thus, the snow depth on the second day is already considerably smaller than in CLASS. By day 19 the snow amount has decreased below 10 kg m^{-2}, and X_s therefore falls below 100% (equation (43)); by the end of the month the snow pack is gone. Evaporation (sublimation) remains consistently high throughout the month, reaching a total of 47 mm, because the snow pack provides a constant water source, and because sublimation is also allowed to occur from the soil ice reservoir. The sublimation rate increases slightly toward the end of the month as $T(0)$ increases with the accelerating disappearance of the snow pack. Runoff remains at zero since the soil is unsaturated. In contrast, the snow pack in CLASS loses only two-thirds of its mass over the entire month, reaching a final value of 13 kg m^{-2}. The fractional snow cover X_s falls below 100 per cent on day 10, but is still as high as 43 per cent on day 30. The evaporation rate is fairly large at first but slowly drops off as the soil is exposed, since unlike the formulation in the old scheme, subsurface ice is not considered in the calculation of Q_E. (This is a more realistic approach, as the sublimation rate of ground ice depends on the soil vapour diffusion rate, which is small in magnitude and moreover reverses its direction daily with the changing sign of the vertical temperature gradient.) The total evaporation is thus only 27 mm. Runoff continues throughout the month from the unfrozen third soil layer, reaching a total of 9 mm.

The resultant daily average energy balance terms are shown in Figure 11. For the old scheme, over most of the month after the first anomalous day the fluxes remain relatively constant, their trends reflecting the aging of the snow pack and the gradual decrease of X_s; after day 26 the rates of change are accelerated owing to the sharp decrease of total albedo, as explained above. The fluxes generated by CLASS exhibit somewhat more complex variations. The magnitude of K_* increases gradually with the decrease in snow albedo during the 10 days of complete snow cover, and more quickly thereafter as soil is gradually exposed. As outlined above, Q_E increases for the first 10 days with $T(0)$ and then gradually decreases. The other fluxes consistently follow the variations in $T(0)$, which peaks on day 15 and at the end of the month. Since the snow packs in the two models dissipate at different rates, it is instructive to compare the relative magnitudes of the energy balance terms on the days when X_s for both models is 43 per cent, i.e. on day 30 for CLASS and on day 26 for the old scheme (Table II). It is clear that the most striking differences are found between the predicted values of K_*, Q_H, and Q_E. The lower value of K_* for the old scheme is due to the fact that at the current snow amount of 2 kg m^{-2}, the calculated snow depth is just above the snow masking depth (0·01 m for bare soil). For the purposes of the surface albedo calculation (equation (47)), therefore, the ground is still assumed to be snow-covered. The differences between the values of Q_H and Q_E produced by the two models are caused by the fact that the old scheme regards the frozen soil as a source of evaporable water, while CLASS does not. Thus, the relative magnitudes of Q_H and Q_E are reversed, as in run 2.

4.4. Run 4: Melting snow on frozen ground

The last run to be considered here compares the model results for a melting snow cover. As in run 3, a snow pack of 40 kg m^{-2} and a constant soil temperature of 0°C are used to initialize the model; in this case, however, the pack is assumed to be fully aged and all the soil water except 4 per cent by volume (the residual amount) is specified as frozen. Figures 12 and 13 show the hydrological terms and the variations in soil moisture content over the month. Once again, it is evident that phase changes proceed much more rapidly in the old scheme than in CLASS. In the old scheme the snow cover is gone by the third day, and the soil has

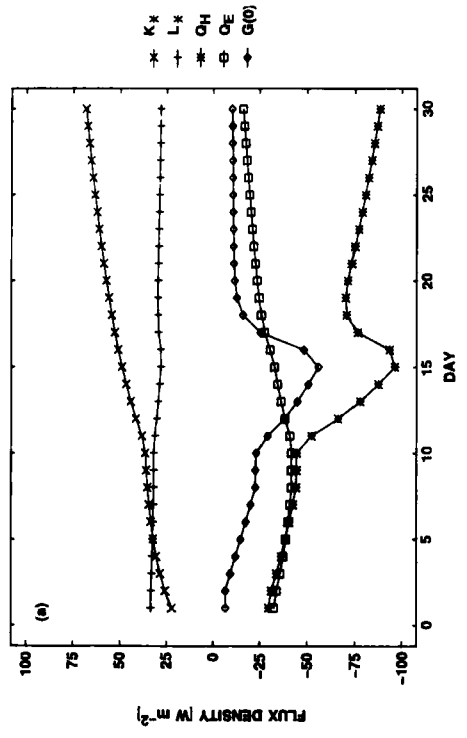

Figure 11. Run 3—Daily average energy balance terms: (a) CLASS; (b) old scheme

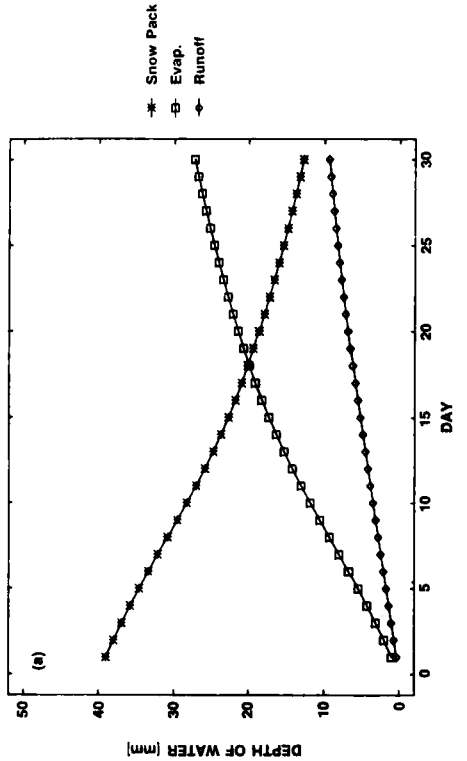

Figure 10. Run 3—Snow pack water equivalent and cumulative values of hydrological terms: (a) CLASS; (b) old scheme

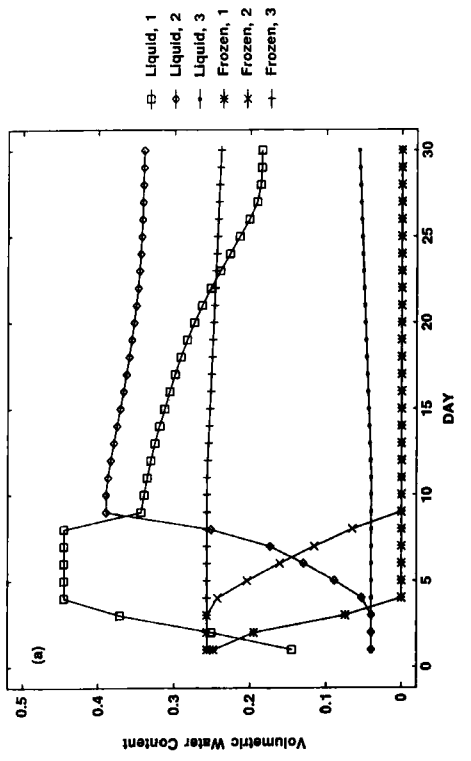

Figure 13. Run 4—Variations in soil moisture content: (a) CLASS; (b) old scheme

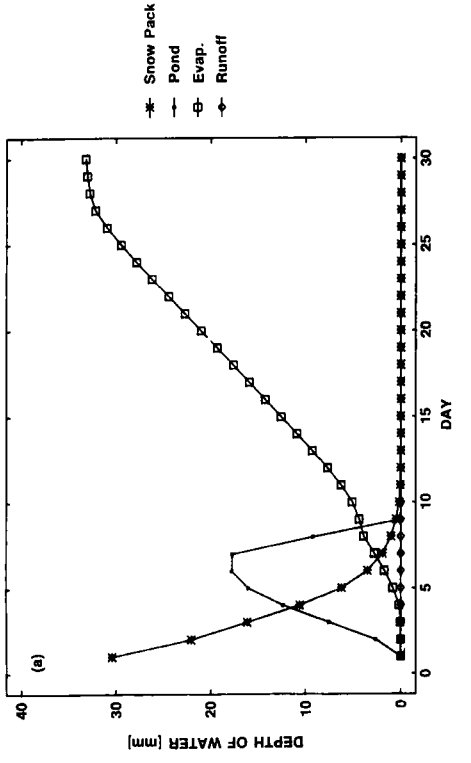

Figure 12. Run 4—Snow pack water equivalent, depth of pond (if present) and cumulative values of hydrological terms: (a) CLASS; (b) old scheme

Table II. Daily average energy balance terms generated by the two models, when snow cover = 43 per cent in run 3

	CLASS	Old scheme
K_*	69	48
L_*	29	33
Q_H	−90	−35
Q_E	−17	−46
$G(0)$	−10	0

thawed completely by the eighth day. By contrast, in CLASS the snow cover takes 10 days to disappear, and although the first and second soil layers are thawed by the fourth and ninth days, respectively, the third layer remains frozen much longer, $\bar{\theta}_f$ decreasing by only 0·02 over the month. Thus, for different reasons, runoff is zero in both models: in CLASS because the liquid water content and therefore the hydraulic conductivity of the lowest layer remain small, and in the old scheme because the soil never reaches saturation.

The melt-water generated by the snow pack is added to the soil liquid moisture store in the old scheme, increasing $\bar{\theta}_l$ by 0·08 over the first 3 days. While the soil is thawing $\bar{\theta}_l$ increases further to a total of 0·38, and thereafter decreases due to evaporation. Evaporation is suppressed for the first 8 days, since while the soil is thawing $T(0)$ is held at 0°C, causing stable conditions to prevail. Afterwards the evaporation rate is high, because the soil is close to saturation. For CLASS, however, the melting of the snow cover leads to saturation of the top soil layer and to ponding of water on the surface. The pond continues to grow until the eighth day, when infiltration begins to occur rapidly, followed by drainage of the top soil layer; this is due to the increasing liquid water content of the second soil layer caused by percolation from above and thawing, which results in a dramatic increase in its hydraulic conductivity. For the rest of the month, evaporation from the first layer and percolation from the first and second layers gradually deplete $\bar{\theta}_l$ for the two layers; by the end of the month, it is evident that $\bar{\theta}_l$ for the first layer has dropped to a low enough level to begin inhibiting evaporation. Because of this drop, and because $T(0)$ in CLASS does not rise as quickly as in the old scheme when the top layers are thawed, the cumulative evaporation for CLASS is slightly less than in the old scheme, even though its evaporation begins earlier; the two model totals for the month are 33 and 37 mm, respectively.

The energy balance terms for the last day of the month are shown in Figure 14. Once again, it is evident that the slow decrease of $\bar{\theta}_l$ in the old scheme has caused a reversal of the magnitudes of Q_H and Q_E between the two models; for CLASS, the fluxes peak at 117 and 35 W m^{-2}, respectively, while for the old scheme the peak values are 7 and 151 W m^{-2}. The early morning sharp rise of $G(0)$ and the delayed increase of Q_H and Q_E are apparent, as in run 1; the characteristic damping of $T(0)$ associated with the force–restore approach is here enhanced by the high soil moisture content. Figure 15 shows the diurnal variations of soil temperatures for the two models. It can be seen that in the old scheme, $T(0)$ shows a marked tendency to oscillate around T_a, an effect which, as noted in section 4.1, can lead to wild fluctuations in Q_H and Q_E. In this run, the oscillation leads to 'wobbles' in Q_H, Q_E, and $G(0)$ between 1400 and 1600 h, and also to sizeable heat fluxes in the middle of the night when unstable conditions are inadvertently set up. CLASS, in contrast, displays none of these anomalies.

5. SUMMARY AND CONCLUSIONS

A new, physically based land surface scheme has been introduced, suitable for incorporation into GCMs. Four 1-month-long test runs were carried out in stand-alone mode, and the model results were compared with those of a simpler scheme that uses the force–restore approach for the calculation of surface temperature and a 'bucket' formulation for soil moisture.

It is evident that the differences in complexity between the two models can give rise to substantial divergence between their results. In the case of the thermal regime, the explicit time stepping used in the old

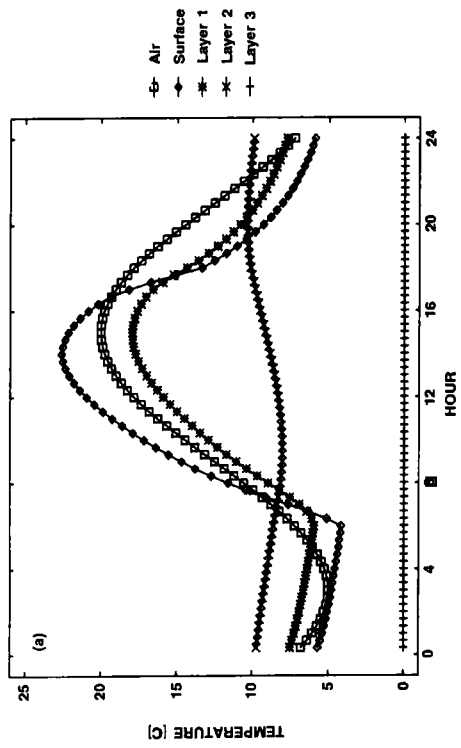

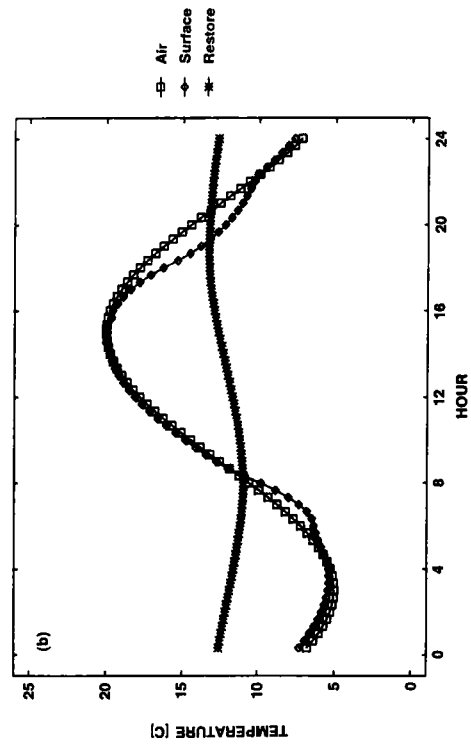

Figure 15. Run 4—Soil and air temperatures for the last day: (a) CLASS; (b) old scheme

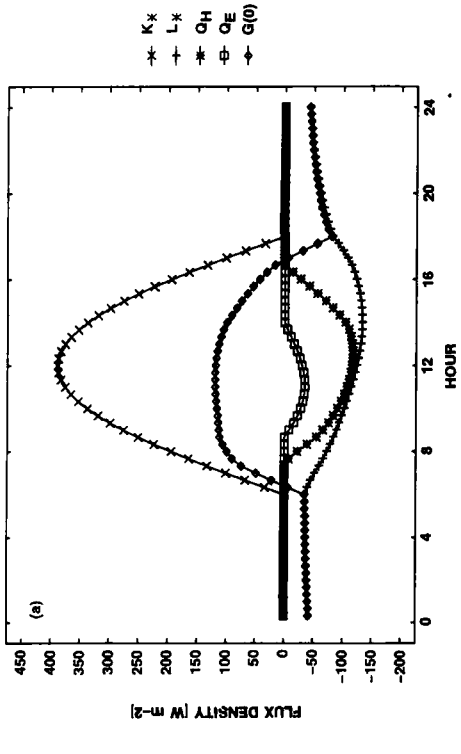

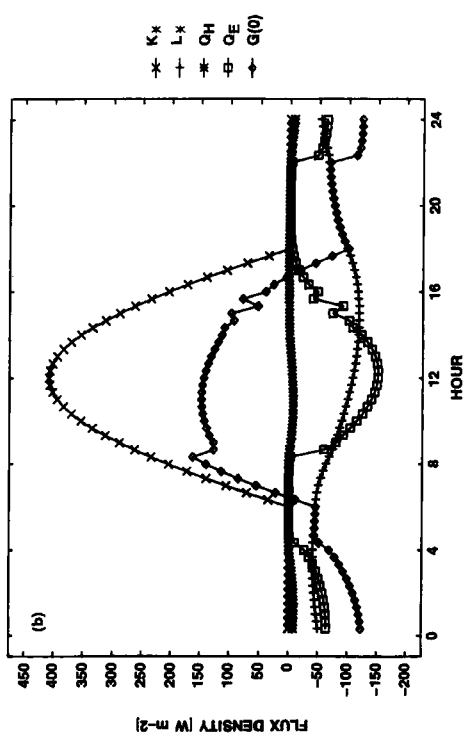

Figure 14. Run 4—Energy balance terms for the last day: (a) CLASS; (b) old scheme

scheme and the fact that only one 'subsurface' temperature is modelled causes the surface temperature to respond rather slowly to diurnal forcing, leading to a damping of the sensible and latent heat fluxes. These factors may also cause the latter to oscillate around the air temperature when the soil is relatively wet and subjected to strong heating. Conversely, owing to neglect of the effects of long-term changes in heat storage, the surface temperature responds relatively quickly to forcings of the order of days or weeks.

For the moisture regime, the fact that only the average moisture content of a single soil layer is modelled causes an insensitivity of the soil moisture content and therefore of the evaporation rate to the removal or addition of water at the surface. Also, the designation of both liquid and frozen soil water as sources for evaporation results in high rates of water loss over frozen ground, and the lack of a drainage parameterization can lead to comparatively large soil moisture contents. Finally, the lumped modelling of soil and snow cover can cause very high snow dissipation rates. Some of the above problems could be corrected quite easily, e.g. by suppressing evaporation from frozen soil water and by parameterizing some value for the drainage rate from the bottom of the bucket; others are unfortunately directly related to the one-layer formulation of the model, and/or to the time stepping.

Some further development work will be required when CLASS is coupled to the CCC GCM. Lateral flow of ground water will have to be parameterized using lumped values of surface slope and depth to bedrock. In the cases of impermeable and/or steeply sloping surfaces, overland flow will have to be allowed. The problem of convective precipitation, which does not cover an entire grid square, will have to be addressed. Test runs of CLASS against field measurements would be helpful, in order to verify some aspects of the model formulation. For example, the slow response time of the third soil layer suggests that its depth should perhaps be decreased, in order to avoid unrealistically long freezing and thawing periods. Finally, the current calculation of fractional snow cover should also be checked as to its applicability on the scale of a GCM grid square. Such studies will be the subject of future papers.

ACKNOWLEDGEMENT

This research was carried out under the tenure of a Natural Sciences and Engineering Research Council Visiting Fellowship.

REFERENCES

Abramopoulos, F., Rosenzweig, C. and Choudhury, B. 1988. 'Improved ground hydrology calculations for global climate models (GCMs): Soil water movement and evapotranspiration', *J. Climate*, **1**, 921–941.

Aguado, E. 1985. 'Radiation balances of melting snow covers at an open site in the central Sierra Nevada, California', *Water Resour. Res.*, **21**, 1649–1654.

Barnett, T. P., Dümenil, L., Schlese, U., Roeckner, E. and Latif, M. 1989. 'The effect of Eurasian snow cover on regional and global climate variations', *J. Atmos. Sci.*, **46**, 661–685.

Bohren, C. F. and Barkstrom, B. R. 1974. 'Theory of the optical properties of snow', *J. Geophys. Res.*, **79**, 4527–4535.

Bouwer, H. 1966. 'Rapid field measurement of air entry value and hydraulic conductivity of soil as significant parameters in flow system analysis', *Water Resour. Res.*, **2**, 729–738.

Camillo, P. J., Gurney, R. J. and Schmugge, T. J. 1983. 'A soil and atmospheric boundary layer model for evapotranspiration and soil moisture studies', *Water Resour. Res.*, **19**, 371–380.

Carson, D. J. 1986. *Parameterizations of Land-surface Processes in Meteorological Office Numerical Weather Prediction and Climate Models*, Meteorological Office, Bracknell, DCTN 37, 54 pp.

Clapp, R. B. and Hornberger, G. M. 1978. 'Empirical equations for some soil hydraulic properties', *Water Resour. Res.*, **14**, 601–604.

Cosby, B. J., Hornberger, G. M., Clapp, R. B. and Ginn, T. R. 1984. 'A statistical exploration of the relationships of soil moisture characteristics to the physical properties of soils', *Water Resour. Res.*, **20**, 682–690.

Deardorff, J. W. 1978. 'Efficient prediction of ground surface temperature and moisture, with inclusion of a layer of vegetation', *J. Geophys. Res.*, **83**, 1889–1903.

Dickinson, R. E. 1988. 'The force–restore model for surface temperatures and its generalizations', *J. Climate*, **1**, 1086–1097.

Dickinson, R. E., Henderson-Sellers, A., Kennedy, P. J. and Wilson, M. F. 1986. *Biosphere–Atmosphere Transfer Scheme (BATS) for the NCAR Community Climate Model*, National Center for Atmospheric Research, Boulder, CO, NCAR/TN-275+STR, 69 pp.

Dirmhirn, I. and Eaton, F. D. 1975. 'Some characteristics of the albedo of snow', *J. Appl. Meteorol.*, **14**, 375–379.

Farouki, O. T. 1981. 'The thermal properties of snow in cold regions', *Cold Regions Sci. Technol.*, **5**, 67–75.

Gallimore, R. G. and Kutzbach, J. E. 1989. 'Effects of soil moisture on the sensitivity of a climate model to earth orbital forcing at 9000 YR BP', *Climatic Change*, **14**, 175–205.

Gold, L. W. 1958. 'Changes in a shallow snow cover subject to a temperate climate', *J. Glaciol.*, **3**, 218–222.
Green, W. H. and Ampt, G. A. 1911. 'Studies on soil physics: I. Flow of air and water through soils', *J. Agr. Sci.*, **4**, 1–24.
Grenfell, T. C. and Maykut, G. A. 1977. 'The optical properties of ice and snow in the Arctic Basin', *J. Glaciol.*, **18**, 445–463.
Hansen, J., Russell, G., Rind, D., Stone, P., Lacis, A., Lebedeff, S., Ruedy, R. and Travis, L. 1983. 'Efficient three-dimensional global models for climate studies: Models I and II', *Mon. Wea. Rev.*, **111**, 609–662.
Hunt, B. G. 1985. 'A model study of some aspects of soil hydrology relevant to climate modelling', *Quart. J. R. Meteorol. Soc.*, **111**, 1071–1085.
Idso, S. B., Jackson, R. D., Reginato, R. J., Kimball, B. A. and Nakayama, F. S. 1975. 'The dependence of bare soil albedo on soil water content'. *J. Appl. Meteorol.*, **14**, 109–113.
Johansen, O. 1975. *Thermal conductivity of soils*', PhD thesis, Trondheim.
Lin, J. D. 1980. 'On the force–restore method for prediction of ground surface temperature', *J. Geophys. Res.*, **85** (C6), 3251–3254.
Longley, R. W. 1960. 'Snow depth and snow density at Resolute, Northwest Territories', *J. Glaciol.*, **3**, 733–738.
Mahrt, L. and Pan, H. 1984. 'A two-layer model of soil hydrology', *Boundary-Layer Meteorol.*, **29**, 1–20.
McCumber, M. C. and Pielke, R. A. 1981. 'Simulation of the effects of surface fluxes of heat and moisture in a mesoscale numerical model', *J. Geophys. Res.*, **86**, 9929–9938.
McFarlane, N. A. and Laprise, R. 1985. *Parameterization of Sub-grid Scale Processes in the AES/CCC Spectral GCM*, Atmospheric Environment Service, Downsview, Ontario, No. 85-12 CCRN 17, 70 pp.
McFarlane, N. A, Boer, G. J., Blanchet, J.-P. and Lazare, M. 1990. 'The Canadian Climate Centre second generation general circulation model and its equilibrium climate', to be submitted.
Meehl, G. A. and Washington, W. M. 1988. 'A comparison of soil-moisture sensitivity in two global climate models', *J. Atmos. Sci.*, **45**, 1476–1492.
Mein, R. G. and Larson, C. L. 1973. 'Modeling infiltration during a steady rain', *Water Resour. Res.*, **9**, 384–394.
Mellor, M. 1977. 'Engineering properties of snow', *J. Glaciol.*, **19**, 15–66.
Mitchell, J. F. B. and Warrilow, D. A. 1987. 'Summer dryness in northern mid-latitudes due to increased CO_2', *Nature*, **330**, 238–240.
Mualem, Y. 1976. 'A new model for predicting the hydraulic conductivity of unsaturated porous media', *Water Resour. Res.*, **12**, 513–522.
Neuman, S. 1976. 'Wetting front pressure head in the infiltration model of Green and Ampt', *Water Resour. Res.*, **12**, 564–566.
Noilhan, J. and Planton, S. 1989. 'A simple parameterization of land surface processes for meteorological models', *Mon. Wea. Rev.*, **117**, 536–549.
Robinson, D. A. and Kukla, G. 1984. 'Albedo of a dissipating snow cover', *J. Clim. Appl. Meteorol.*, **23**, 1626–1634.
Sellers, P. J., Mintz, Y., Sud, Y. C. and Dalcher, A. 1986. 'A simple biosphere model (SiB) for use within general circulation models', *J. Atmos. Sci.*, **43**, 505–531.
Thomas, C. W. 1963. 'On the transfer of visible radiation through sea ice and snow', *J. Glaciol.*, **4**, 481–484.
Van de Griend, A. A. and van Boxel, J. H. 1989. 'Water and surface energy balance model with a multilayer canopy representation for remote sensing purposes', *Water Resour. Res.*, **25**, 949–971.
Van Wijk, W. R. and de Vries, D. A., 1963. 'Periodic temperature variations in a homogeneous soil', in van Wijk, W. R. (ed.), *Physics of Plant Environment*, North-Holland, Amsterdam.
Washington, W. M. and Meehl, G. A. 1986. 'General circulation model CO_2 sensitivity experiments: snow-sea ice albedo parameterizations and globally averaged surface air temperature', *Climatic Change*, **8**, 231–241.
Wilson, M. F. and Henderson-Sellers, A. 1985. 'A global archive of land cover and soils data for use in general circulation climate models', *J. Climatol.*, **5**, 119–143.
Yamazaki, K. 1989. 'A study of the impact of soil moisture and surface albedo changes on global climate using the MRI GCM-I', *J. Meteorol. Soc. Jpn*, **67**, 123–146.
Yee, S. Y. K. 1988. 'The force–restore method revisited', *Boundary-Layer Meteorol.*, **43**, 85–90.